Low Density Supersonic Decelerator Flight Dynamics Test - 1 Flight Design and Targeting

Mark Ivanov, Jet Propulsion Laboratory, 4800 Oak Grove Drive, Pasadena, CA.

Abstract

NASA's Low Density Supersonic Decelerator (LDSD) program was established to identify, develop, and eventually qualify to Test Readiness Level (TRL) - 6 aerodynamic decelerators for eventual use on Mars. Through comprehensive Mars application studies, two distinct SIAD designs were chosen that afforded the optimum balance of benefit, cost, and development risk. In addition, a Supersonic Disk Sail (SSDS) parachute design was chosen that satisfied the same criteria. The final phase of the multi-tiered qualification process involves Earth Supersonic Flight Dynamics Tests (SFDTs) within environmental conditions similar to those that would be experienced during a Mars Entry, Descent, and Landing (EDL) mission. The first of these flight tests (i.e. SFDT-1) was completed on June 28, 2014 with two more tests scheduled for the summer of 2015 and 2016, respectively. The basic flight design for all the SFDT flights is for the SFDT test vehicle to be ferried to a float altitude of 120kft by a 34Mcf heavy lift helium balloon. Once float altitude is reached, the test vehicle is released from the balloon, spun-up for stability, and accelerated to supersonic speeds using a Star48 solid rocket motor. After burnout of the Star48 motor the vehicle decelerates to pre-flight selected test conditions for the deployment of the SIAD system. After further deceleration with the SIAD deployed, the SSDS parachute is then deployed stressing the performance of the parachute in the wake of the SIAD augmented blunt body. The test vehicle/SIAD/parachute system then descends to splashdown in the Pacific Ocean for eventual recovery. This paper will discuss the development of both the test vehicle and the trajectory sequence including design trade-offs resulting from the interaction of both engineering efforts. In addition, the SFDT-1 nominal trajectory design and associated sensitivities will be discussed as well as an overview of the on-board flight software used to trigger and sequence the main flight events necessary to deploy the deceleration technologies. Finally, as-flown performance of the SFDT-1 system will be discussed.

I. Introduction

The Low Density Supersonic Decelerator (LDSD) project was established to identify, develop, and eventually qualify aerodynamic decelerators for eventual use on Mars. Decelerator technologies assessed were related to Supersonic Inflatable Aerodynamic Decelerators (SIADs) as well as supersonically deployed parachutes. Through comprehensive Mars application studies, two distinct SIAD designs were chosen that afforded the optimum balance of benefit, cost, and development risk (Figure 1). In addition, a Supersonic Disk Sail (SSDS) parachute design was chosen that satisfied the same criteria (Figure 2). The final phase of the on-going multi-tiered qualification process involves Earth Supersonic Flight Dynamics Tests (SFDTs) within environmental conditions similar to that which would be experienced during a Mars Entry, Descent, and Landing (EDL) mission. The first flight test (i.e. SFDT-1) was completed on June 28, 2014 with two remaining tests scheduled for the summer of 2015 and 2016, respectively. It can be assumed that the basic elements of the vehicle configuration and mission design described herein for SFDT-1 will be directly applicable to any follow-on test flights.

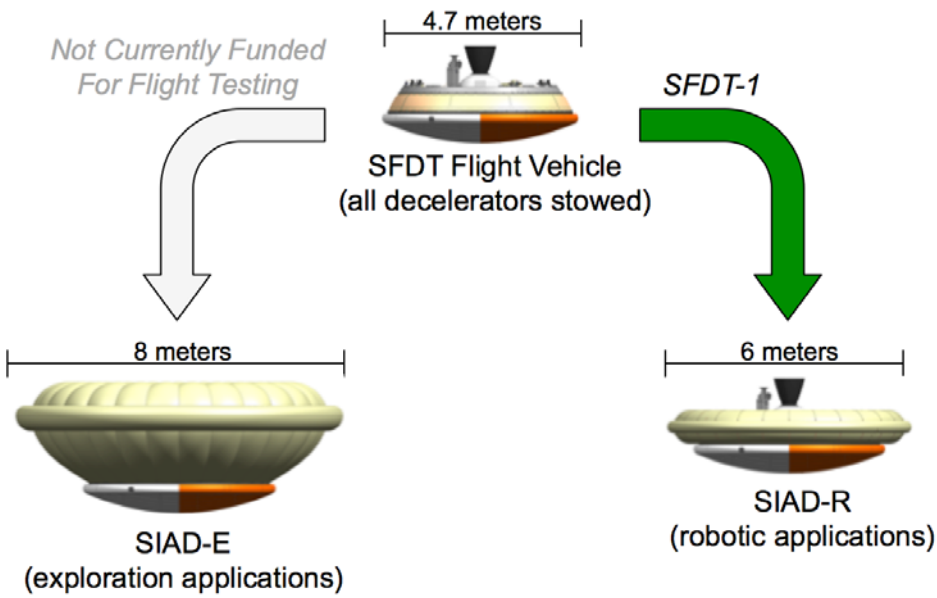

Figure 1: LDSD SIAD Configurations

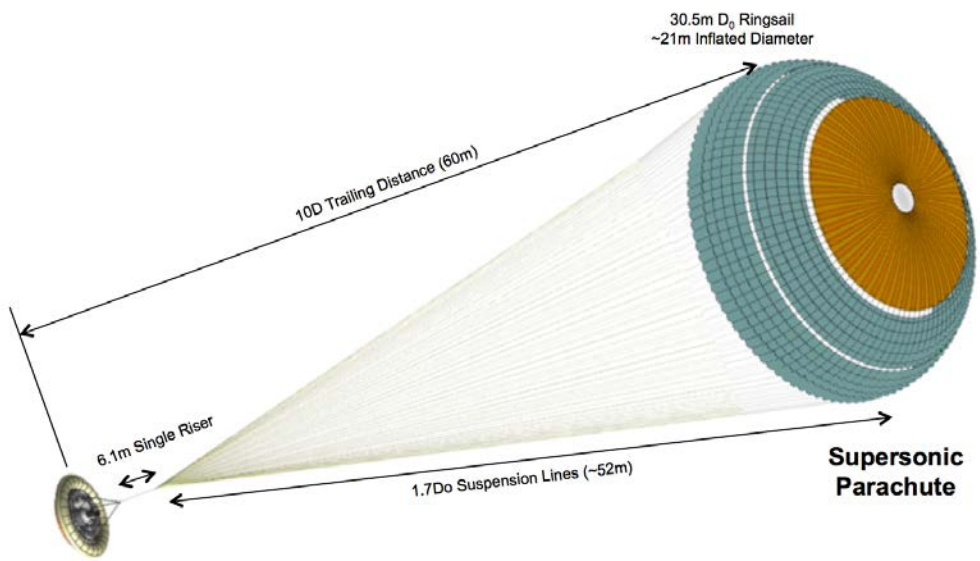

Figure 2: LDSD Supersonic Parachute

Delivery of both technology components under development (SIAD and parachute) to their unique Mars test conditions for SFDT-1 involved developing a low cost delivery system, a robust mission design as studied through pre-flight trajectory simulations, and on-board triggering software required to sequence the mission flight events leading to deployment of the deceleration technologies. An overview of the SFDT-1 mission design is shown in Figure 3. Pre-flight trajectory simulations supporting the development of the flight vehicle, the flight events, and flight software triggering logic were accomplished utilizing the Jet Propulsion Laboratory (JPL) flight dynamics tool Dynamics Simulator for Entry, Descent and Surface landing (DSENDS, Ref 7). The on-board triggering logic was designed jointly between JPL and the Wallops Flight Facility (WFF), coding and modular level testing was performed by WFF, and final system

level testing performed by JPL. The triggering logic architecture represents a generalized solution enabling unique tailoring of the triggering criteria for any desired number of triggered flight events.

The sections that follow will focus on the flight simulation effort in support of the SFDT-1 flight test with an emphasis on 1) the development of the flight vehicle, 2) the simulated environment models, 3) uncertainty analysis leading to the variability of the test conditions, and the 4) targeting process culminating with the actual flight operation. Further, the basic functionality of the triggering software will also be discussed to provide insight regarding the flight constants generated during the targeting process.

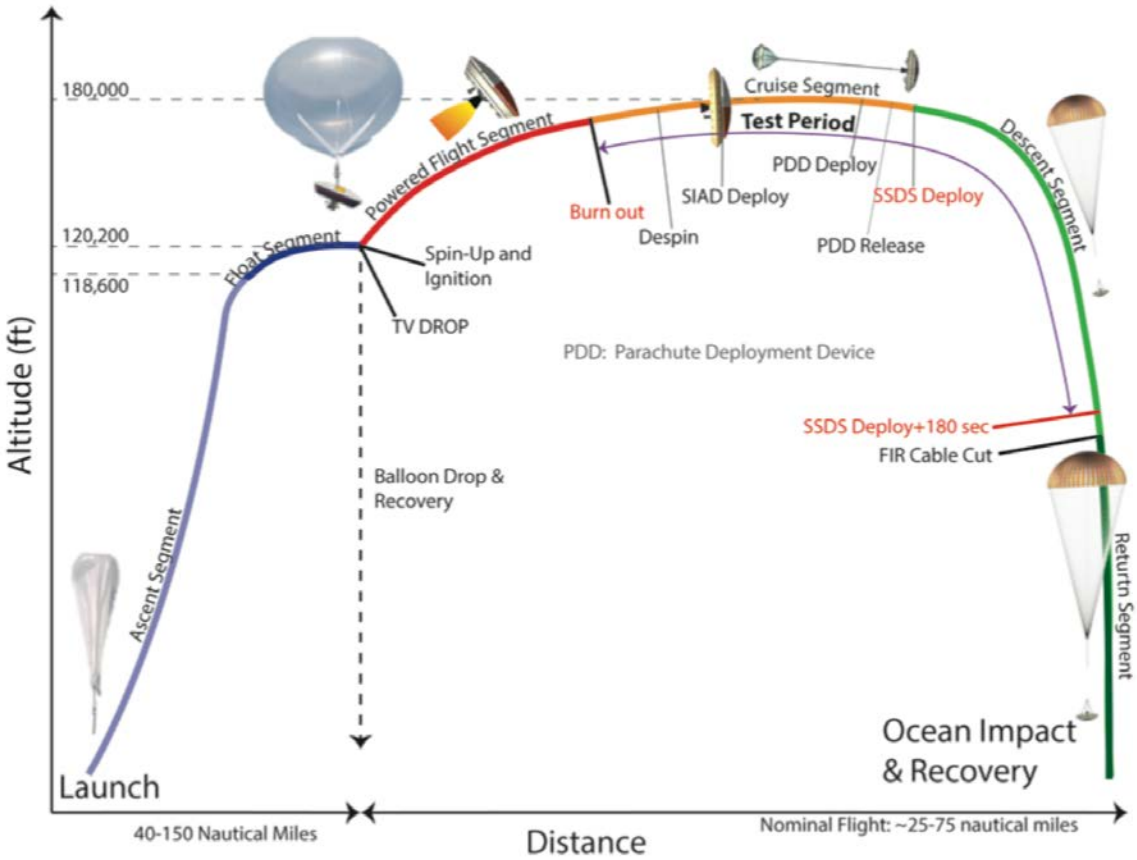

Figure 3: LDSD Balloon and Test Vehicle Mission Profiles

II. JPL Flight Simulation Toolkit: DSENDS

The DSENDS flight simulation program was developed at JPL and is capable of modeling complexity ranging from simple systems with three degrees-of-freedom (DOF) dynamics, all the way to multi-body, flexible-body systems with dynamics involving hundreds and even thousands of DOF. In addition to the dynamics simulation, DSENDS also provides models of the on-board devices and environment effects. DSENDS is built upon a multi-mission spacecraft simulation toolkit which was also developed at JPL. The tool-kit implements a state-of-the-art dynamics engine, Dynamics Algorithms for Real-Time Simulation (DARTS), which provides for "order n" computational performance of complex multi-body systems with flexible internal modes. An extensive model library exists for sensors, actuators, environments, environment interaction, and avionics elements. In addition a number of common guidance and control functions are available as models to allow stub-based closing-of-the-loop even in the absence of an externally provided G&C model. Models in arbitrary numbers can be instantiated in any DSENDS deployment allowing for simultaneous operation of multiple flight vehicles. The DSENDS architecture is

open allowing for easy linking of third-party codes as shared-object libraries, general source code (e.g. C/C++, Fortran), MATLAB scripts, or as Python modules.

For the LDSD application, the DSENDS simulation complexity matured over time from simple models in support of initial pre-design studies to high fidelity 6DOF dynamics requiring detailed modeling of the significant performance contributors. Figure 4 depicts the various models utilized in the 6DOF DSENDS simulation. Note that simulation validation was accomplished using the NASA Langley Research Center (LaRC) flight dynamics tool Program to Optimize Simulated Trajectories II (POST2, Ref 8). Approximately 250 parameters associated with these models were varied to conduct Monte Carlo analyses to study the statistical variability in the vehicle dynamics and trajectory profile. The Monte Carlo effort will be discussed in more detail later.

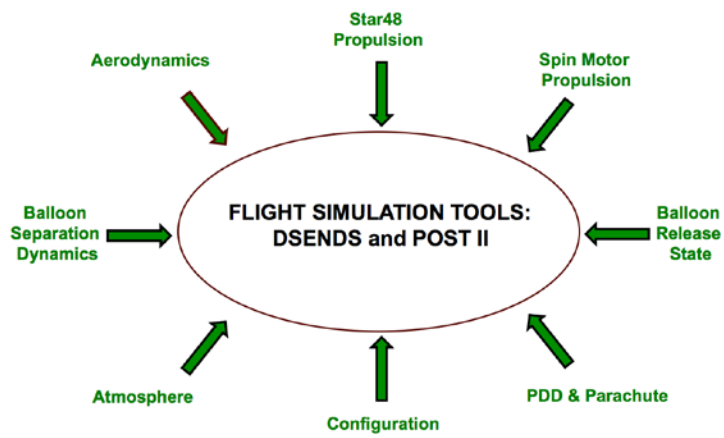

Figure 4: LDSD Unique Modeling Overview

III. Concurrent SFDT Hardware and Trajectory Design Process

A. Flight Test Requirements

The flight test requirements for SFDT-1 manifest from the overall test architecture. The test architecture consists of the "five pillars of qualification" for deployable aerodynamic decelerators (Ref 1):

Phase 1. Initial Deployment
Phase 2. Inflation Dynamics
Phase 3. Peak Strength
Phase 4. Supersonic Performance
Phase 5. Subsonic Performance

The entire flight test campaign was designed to primarily address Phases 2, 4, and 5. To this end, a test vehicle had to be developed capable of achieving the derived environmental conditions and constraints shown in Table 1. These requirements resulted from extensive studies on both the type as well as the operating environment of deployable aerodynamic decelerators to enhance the performance of Mars entry probes (Ref 3). The common conclusion from these studies was that enhanced aerodynamic deceleration beginning around Mach 4 could significantly improve altitude, landed mass, and/or accuracy performance. Since parachute technology is limited by heating above approximately Mach 2.5, the more heat resilient SIAD technology could be deployed above this Mach regime followed by the deployment of a large diameter parachute at speeds <= Mach 2.5. Note that the implementation of both SIAD and parachute technologies in a single mission design was critical in achieving the maximum performance benefits resulting from the studies and shaped the Earth test flight configuration and test requirements.

Table 1: LDSD Earth Test Flight Requirements

Flight Requirements	Value
SIAD Deploy Mach ***Target***	3.5 to 3.8
SIAD Chute Line Stretch Mach ***Target***	2.2 to 2.50
SIAD Deploy Scaled Mars Altitude ***Target***	5 to 25 km
SIAD Deploy Mach Error	+/- 0.25
Chute Line Stretch Mach Error	+/- 0.25
Min Dynamic Pressure At Chute Line Stretch	>= 240 Pa
Max Chute Inflation Load	<= 80 klbf
Max AoA From SIAD Deploy To Chute Line Stretch	<= 25 deg
SIAD Deployment Max Dynamic Pressure	<= 2000 Pa
Max Residual Spin Rate After Spin Down	<= 20 deg/sec
Max AoA From SIAD Deploy To PDD Trigger	<= 20 deg
Max Delta Density From SIAD Deploy to SIAD Deploy + 10 sec	<= 10^{-4} kg/m^3
Min Time From SIAD Deploy to PDD Trigger	>= 10 sec

Translating the Mars flight requirements to equivalent Earth flight conditions was necessary to understand the flight envelope the test vehicle would have to achieve. Of the two target conditions at SIAD deployment (i.e. Mach and Mars altitude) equating Mars altitude to Earth altitude required more consideration. As will be discussed in the hardware design process, there was a mass limitation of the test vehicle due to the reliance on the use of a heavy lift high altitude balloon to ferry the vehicle to a high, more favorable initial altitude condition. Since the objective of the test was to characterize the flight *dynamics* of an SIAD augmented Mars flight system, mass scaling was necessary to adjust the Earth test altitude to account for a lower mass Earth test vehicle as compared to an expected heavier flight vehicle that ultimately would be used at Mars. The following scaling equation was used to adjust the Mars density to achieve the equivalent Earth test flight density, and subsequent Earth test flight altitude, given the lighter test vehicle (Ref 2):

$$\text{Density At Earth} = \text{Density At Mars} * \text{Earth Test Vehicle Mass} / \text{Mars Vehicle Mass} \quad (1)$$

where:

Density At Mars = density at a chosen Mars altitude between 5 and 25km
Earth Test Vehicle Mass = test vehicle mass at SIAD deployment = 1461kg
Mars Vehicle Mass = assumed future Mars vehicle mass = 4250kg

Atmospheric tables for both Earth and Mars were used to determine the equivalent Earth test flight altitude. For SFDT-1 the Mars altitude target requirement was 17.0 km which translated to an equivalent flight dynamics Earth altitude of 51.7 km.

B. Hardware Design

The basic elements of the Earth trajectory design for SFDT-1 matured in parallel with the test vehicle hardware design. Concurrent engineering between these two disciplines enabled rapid prototyping that eventually culminated into a final design. The creative process for designing the Earth test vehicle focused on producing a simple low cost hardware configuration that could achieve the desired test conditions with 1) flight equivalent Mars dynamic behavior and 2) an acceptable degree of mission success. It was argued that the target mass and the outer mold line were the only elements of a future Mars vehicle that could be characterized with some degree confidence (outer mold line is limited by launch vehicle fairing size informing a target mass limitation due to SIAD augmented blunt body vehicle performance at Mars). This was advantageous since confidence in the outer mold line ensured that aerodynamic characteristics resulting from the Earth test flights could be applied directly to a future Mars mission. Therefore the test vehicle forebody size and shape was constrained to be consistent with the outer mold line of the assumed

future Mars vehicle. As mentioned previously, the total test vehicle mass was allowed to vary within the balloon limitations given the ability to scale the test conditions appropriately.

The acceptable probability of successfully meeting the SFDT-1 target conditions within tolerances was defined to be >= 90% versus the more typical, and challenging, probability of success >= 99.87% (a.k.a. 3 sigma). The lower success criteria enabled the reduction, and in some cases the complete removal, of complex systems that are typically included on an atmospheric flight vehicle capable of achieving specific flight conditions. Subsequent candidate systems for removal were related to Guidance, Navigation, and Control (GNC) and therefore impacted the ability to accurately and reliably achieve the test conditions. However the rapid prototyping process using DSENDS enabled sufficient insight to make hardware trade-offs while still satisfying the defined success criteria. The final test vehicle configuration resulting from the design cycle is shown in Figure 5 and had the following flight performance related attributes:

1) Single stage vehicle
2) Single engine vehicle
3) Spin stabilization during powered phase
4) "Loose" build tolerances
5) No guidance and control hardware (or software)

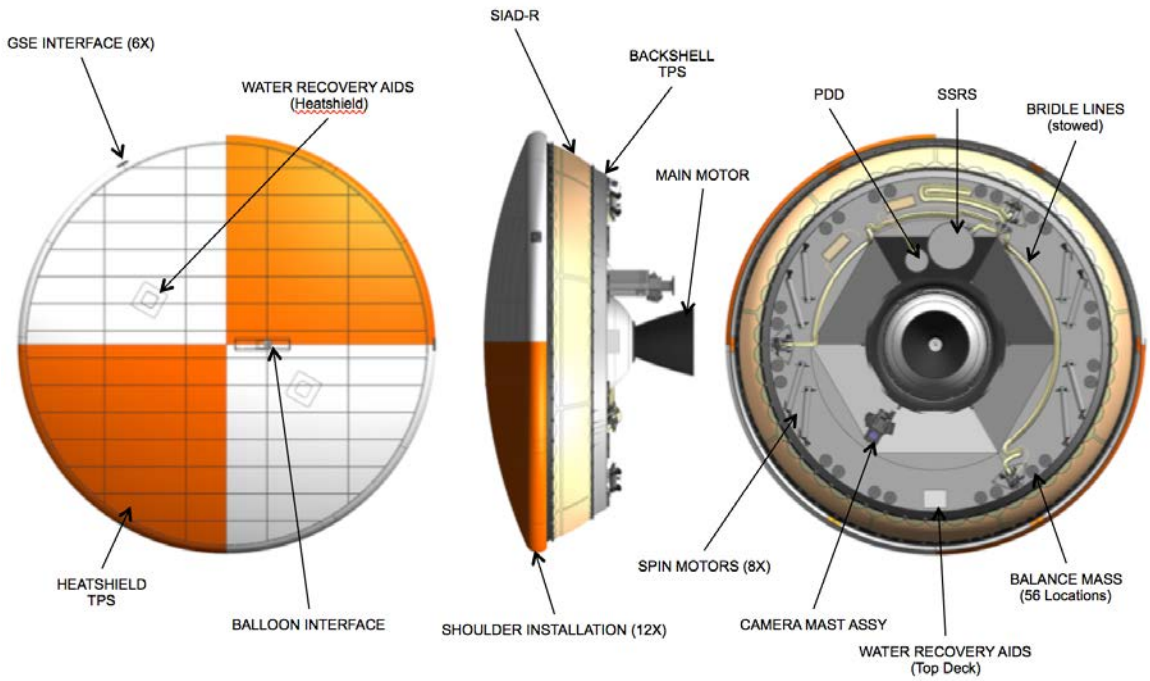

Figure 5: LDSD Test Flight Configuration

Given the high altitude necessary to achieve the test conditions for both decelerators, a multi-stage vehicle would have been necessary to accelerate the test vehicle directly from the ground greatly inflating the cost of the LDSD project. However, a high altitude balloon as a 1st stage substitute enabled low enough energy requirements to require only a single "upper" stage test vehicle design. The high altitude balloon was provided by the Columbia Scientific Balloon Facility (CSBF) and was capable of ferrying an 8000lbs payload to an altitude of ~120kft At that initial altitude the energy needed to accelerate the test vehicle to the required test speed and altitude could be supplied by a single Star48 solid rocket motor, supplied by Alliant Techsystems (ATK).

The Star48 provided more acceleration than necessary from the balloon hand-off altitude, therefore in the interest of reducing the overall mass of the vehicle (i.e. to address the balloon payload mass limitations) the Star48 was offloaded by ~20%—the most offload ever attempted for a Star48. A single engine test vehicle was chosen over multiple engines to not only take advantage of the availability of the Star48 option

providing improved reliability due to its lengthy flight heritage but also to reduce both complexity and stability issues resulting from multi-engine performance differences (canting the thrust vectors of multiple engines to pass through the burnout center of mass proved to complex and costly; Ref 4). From a powered flight perspective the use of a single centerline mounted engine did produce its own residual stability problems resulting from the thrust-induced torques about the center of mass due to misalignments related to the motor mounting, engine bell attachment, thrust direction, and center of mass uncertainties. This was solved by spinning the vehicle at ~50rpm to average out these disturbances. As a beneficial consequence, the spin rate added suitable stability margins to relax some build tolerances related to the Star48 uncertainties previously mentioned as well as the uncertainty of the overall mass properties of the vehicle. From a technology deployment perspective the centerline mounted engine prevented a mortar deployed parachute (as it would be deployed at Mars) due to the destabilizing torque imparted from an off centerline mounted parachute/mortar system. Ultimately much smaller mortar deployed ballute was utilized off centerline to pull the parachute out using aerodynamic force.

Early in the design cycle an additional vehicle control element was considered as related to the spin rate and highlighted a critical flight performance sensitivity. The spin rate provides inertial stiffness through the resultant angular momentum but as the vehicle accelerates during the powered phase the aerodynamic trimming torque soon overcomes this momentum resulting in the vehicle rotating to a trim condition defined by the instantaneous relative velocity vector. It follows that since the Star48 thrust is along a fixed axis of the vehicle the trajectory will be affected by, and found to be sensitive to, the timing of this open-loop trimming behavior. Modulation of the trimming motion during flight could have been possible by adjusting the spin rate (i.e. the angular momentum) thereby enabling limited trajectory control early in the powered phase prior to large aerodynamics forces acting on the vehicle. However to reduced complexity and cost as stated earlier, it was decided to use a fixed spin rate during the powered phase and accept larger trajectory errors (trajectory data will be shown later). The test vehicle spin rate was accomplished using four spin-up motors in concert with four spin-down motors to remove the spin rate prior to deployment of the deceleration technology. Nammo Talley provided the spin motors.

C. Trajectory Design

Key to any trajectory design is defining the sequence of events for the mission. The sequencing of the mission was a direct consequence of the final configuration since a mission sequence is typically reflective of the transitions between hardware states. Table 2 lists the significant flight events comprising the mission sequence. The flight sequence began after an approximately 2hr ascent on the balloon after which the test vehicle along with the embedded deceleration technology was released. Once released, the test vehicle fired the spin up motors and then ignited the Star48 main engine. After an approximately 70sec Star48 powered phase during which the test vehicle increased altitude from ~36km to ~50km, the Star48 burned out triggering the spin down motors to fire followed by the deployment of both the SIAD and subsequently the parachute. Descent on the parachute to splashdown was expected to take approximately 40 minutes.

Table 2: SFDT Mission Sequence

Event	Timing	Description
Pre-Ignition Sequence (DROP):		
Balloon Release	DROP + 0.0sec	Vehicle is released from balloon.
Fire spin-up motors 1 and 3	DROP + 0.3sec	Vehicle begins spin-up.
Fire spin-up motors 2 and 4	DROP + 1.6sec	Vehicle continues spin-up to 50rpm.
Ignite Star48	DROP + 2.1sec	Vehicle begins acceleration.
// Test Vehicle Powered Phase //		
Post Main Engine Burn Sequence (BURNOUT):		Triggered by low acceleration.
Fire spin-down motors 5 and 7	BURNOUT + 1.0sec	Vehicle begins spin-down.
Fire spin-down motors 6 and 8	BURNOUT + 1.5sec	Vehicle continues spin-down to 0rpm.
// Pre-Deployment Coast Phase //		
SIAD Deployment Sequence (SIAD):		Triggered by navigated speed.
Open observation camera covers	SIAD + 0.1sec	Open lens protective covers.
Fire gas inflation generators set 1	SIAD + 2.3sec	Fire 1st grouping of 9 gas generators.
Fire gas inflation generators set 2	SIAD + 2.6sec	Fire 2nd grouping of 9 gas generators.
SIAD Fully Deployed (SD)	SIAD + 3.6sec	SIAD at full inflated integrity.
// SIAD Observation Phase //		
Parachute Deployment Sequence (CHUTE):		Triggered by navigated speed.
Fire PDD mortar	CHUTE + 0.1sec	Deploy ballute to be used for chute extraction.
Extract Parachute (EXTRACT)	CHUTE + 5.0sec	Cut line to allow ballute to extract parachute.
Line Stretch / Begin Parachute Inflation (LINE)	CHUTE + 2.0 to 5.0sec	Timing dependent on dynamic pressure.
Parachute Full Inflated	LINE + 1.0sec	Parachute is at maximum inflation diameter.
// Parachute Observation Phase //		
End Science Observations	EXTRACT + 180.0sec	Decelerator test portion of the flight ends.

Only two transitions within the mission sequence allow for tailoring to a unique set of test conditions: SIAD deployment and parachute deployment speeds. Further tailoring of the overall trajectory profile external to the sequence was afforded by adjusting the elevation, or hang angle, of the vehicle when attached to the balloon prior to drop (Figure 6). The altitude at SIAD deployment was largely a function of the hang angle since increasing or decreasing the hang angle resulted in a more lofted or shallow trajectory, respectively. Speed at burnout was also affected by the hang angle. For example, higher speeds at burnout could be achieved with a more lofted trajectory since lower drag losses ensued from lower atmospheric densities at the higher altitudes that more than compensated for the associated higher gravity losses experienced during the initial climb-out (i.e. drag losses were more sensitive to the trajectory design). By adjusting both the hang angle and SIAD deployment speed simultaneously, the DSENDS simulation could achieve the SIAD target conditions in both Mach and altitude with a high degree of precision. The parachute Mach target was achieved by adjusting only the parachute deployment speed and was treated separately following the convergence of the SIAD target problem when using DSENDS. Both problems were solved through employing a simple 1-dimensional secant search method that ultimately iterated to the required settings for the hang angle, SIAD deployment speed, and parachute deployment speed. Note from Table 2 that for both deployments, several seconds of deployment sequencing actions were required which had to be accounted for when assessing the required triggering speed (i.e. deployment conditions were assessed at the end of the deployment sequence with the sequence being initiated by the trigger criteria).

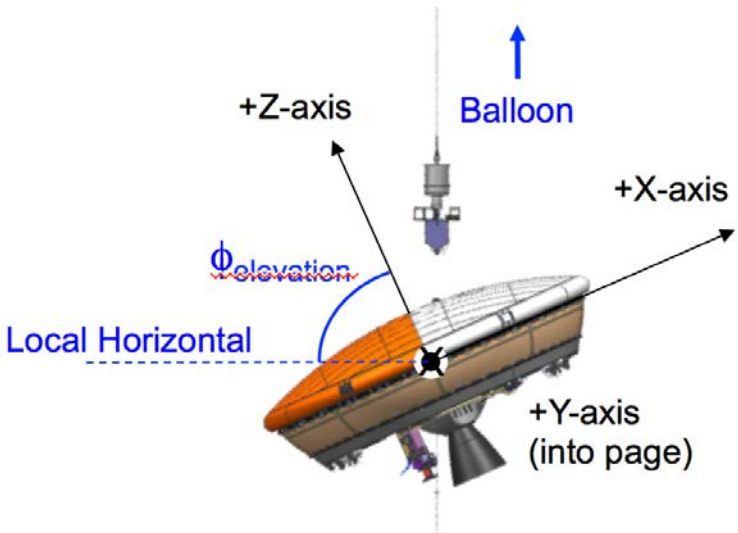

Figure 6: LDSD Test Vehicle Orientation While Connected To Balloon

Sensitivities were explored once the nominal trajectory design was complete. As mentioned earlier, the trajectory during the powered phase was highly sensitive to the rotational dynamics experienced by the vehicle. Figure 7 shows the vehicle pitch angle as well as the relative velocity flight path angle as a function of time (both referenced from the local horizontal). Figure 8 shows the vehicle heading angle as well as the relative velocity flight azimuth as a function of time (both referenced from North). Note from both plots that early in the powered phase the vehicle attitude begins to rotate down and out of plane in reaction to the aerodynamic trimming torque. Both plots also show the eventual oscillatory steady state trimming behavior of the vehicle about the relative velocity vector toward the end of the powered phase. The out of plane rotation is a direct consequence of a spinning object under the influence of an external torque (in this case aerodynamic torque) resulting in gyroscopic precession[1]. Both rotations were found to be very sensitive to the pitch and yaw moment characteristics that were determined through extensive Computational Fluid Dynamics (CFD) analysis (Ref. 5). Additionally, complexity of the powered phase CFD analysis was significantly compounded by the presence of the Star48 thrust plume that highly influenced the flow in the wake of the blunt body configuration. Detailed CFD had never before been performed on a single rocket propelled blunt body configuration and as will be discussed in the as-flown section of this paper, a large unpredicted bias in the aerodynamic moments was observed prompting an even more detailed investigation as a result.

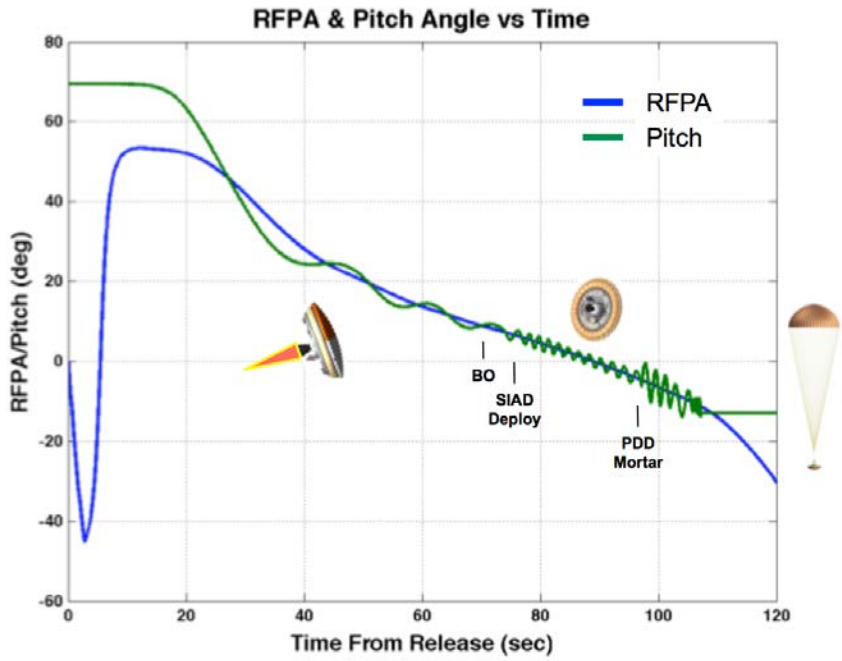

Figure 7: SFDT-1 Test Vehicle Pitch and Flight Path Angle vs Time

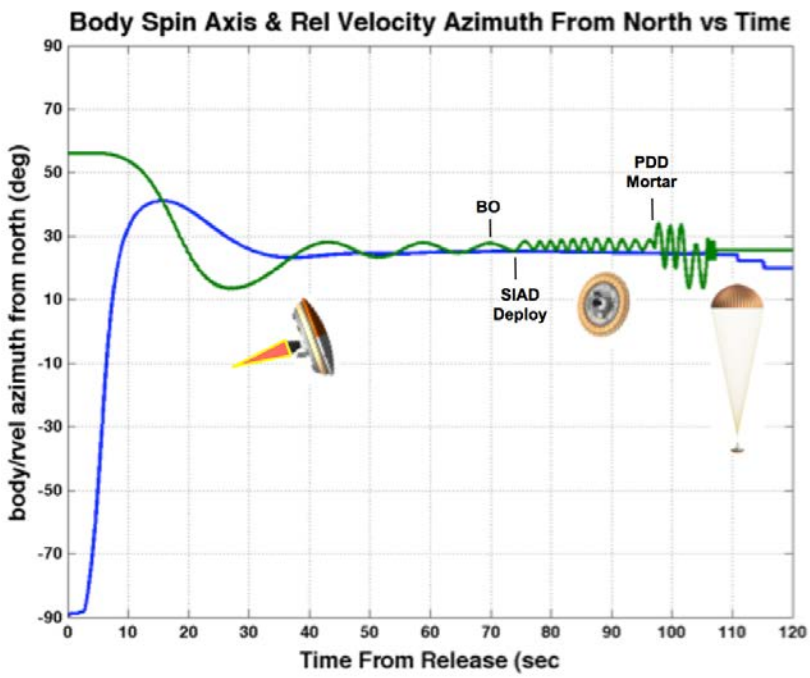

Figure 8: SFDT-1 Test Vehicle Yaw and Flight Azimuth vs Time

Once the simulation was targeted to the correct speeds at the deployment events, the actual flight triggering mechanisms had to be determined. The original idea was NOT to use speed triggers at all but instead use mission time as the triggering mechanism set at a constant value for each deployment. Although not very intuitive, using constant mission time as the trigger for each deployment was very attractive to

reduce complexity and cost since low cost hardware timers could be used with little to no flight software algorithms required for support. However this design produced unacceptable errors in deployment Mach therefore navigated speed became the logical alternative. Using navigated speed as the trigger mechanism inherently provided the ability to adapt to large trajectory profile uncertainty by maintaining speed at the deployment events while also satisfying the Mach requirements even in the presence of speed of sound errors due to the large altitude uncertainties at those events. With regards to achieving the SIAD deployment Mars altitude in flight, the original idea was to use adaptive roll rate control during the powered phase but as mentioned earlier that concept was abandoned due to cost and complexity. As a consequence, it was decided to simply absorb the increase in altitude error by increasing the required accuracy. Software implementation of the triggers will be discussed further later in the paper.

Once the nominal trajectory and triggering mechanisms were established, affects of uncertainty in the foundational simulation models were further studied using a traditional Monte Carlo approach. The Monte Carlo process statistically varied over 250 modeling parameters independently via probability density functions assigned to each individual parameter. A categorization of the parameters varied is shown in Table 3. It was determined that approximately 8000 dispersed simulations were sufficient to accurately characterized the statistical uncertainty in the LDSD flight design. Histograms of the requirements were produced to ensure compliance with the flight requirements as well as inspect for flight performance sensitivities (SFDT-1 unique histograms will be shown subsequently).

Table 3: LDSD Simulation Modeling Uncertainty Summary

Category	Error Source
Mass Properties	Total Dry Mass
Mass Properties	Dry Mass CG Location (x / y / z)
Mass Properties	Dry Moments/Products of Inertia
Mass Properties	Star48 CG Location
Mass Properties	Star48 Mass Properties: Prop, Dry, Burnout, Slag Mass & MOI
Propulsion	Star48 Mounting Tilt Alignment
Propulsion	Star48 Mounting Location
Propulsion	Star48 Thrust Reaction Offset
Propulsion	Star48 Thrust / Isp
Propulsion	Star48 Temperature Variation
Propulsion	Star48 / Spin Motor Thrust Dir
Propulsion	Spin Motor Delay; Burnout; Temp
Propulsion	Spin Motor Impulse
Propulsion	Spin Motors Reaction Location
Aerodynamics	TV/SIAD/Chute Aero / Ballute Aero
Staging	Balloon Release Density
Staging	Release Mech / Pendulum Angle
Staging	Release Azimuth
Staging	Release Mech/Pendulum Rates
Staging	GLN Mac Velocity Error
Staging	PDD Impulse / PDD Ejection Vel
Staging	PDD Reaction Location
Staging	PDD Force Direction
Atmosphere	Atm Density,Temp.Press.Winds

IV. Targeting The SFDT-1 Test Conditions

For SFDT-1, the required test conditions were chosen so that the deceleration technologies where deployed at the highest possible energy states (i.e. speeds) anticipated for future Mars applications. The SFDT-1 target states were as follows: SIAD Mach = 3.8, SIAD Mars Altitude = 17km, Parachute Mach = 2.5. These target parameters were utilized in the trajectory design process previously discussed. Flight software constants were derived from the nominal targeted simulation and will be discussed further in the next section. In addition to Figures 7 and 8 shown previously, Figures 9 through 11 show the nominal predicted altitude vs downrange distance traveled, Mach and dynamic pressure vs time, and longitudinal (thrust axis) sensed acceleration vs time profiles for SFDT-1, respectively. Figures 12, 13, and 14 show the predicted uncertainty for the target test conditions of SIAD deploy Mach, SIAD deploy Mars altitude, and parachute deploy Mach, respectively, that resulted from the Monte Carlo analysis for the SFDT-1 mission. Figure 15 shows the SFDT-1 dynamic pressure vs Mach for the nominal trajectory in relation to the 8000 trajectories resulting from the Monte Carlo analysis. Included in Figure 15 is the SIAD and parachute deployment "boxes" defined by the allowable uncertainty in achieving both test conditions (see Table 1 for allowable uncertainties) with supporting iso-contour lines of Earth altitude, Mars altitude, and chute load.

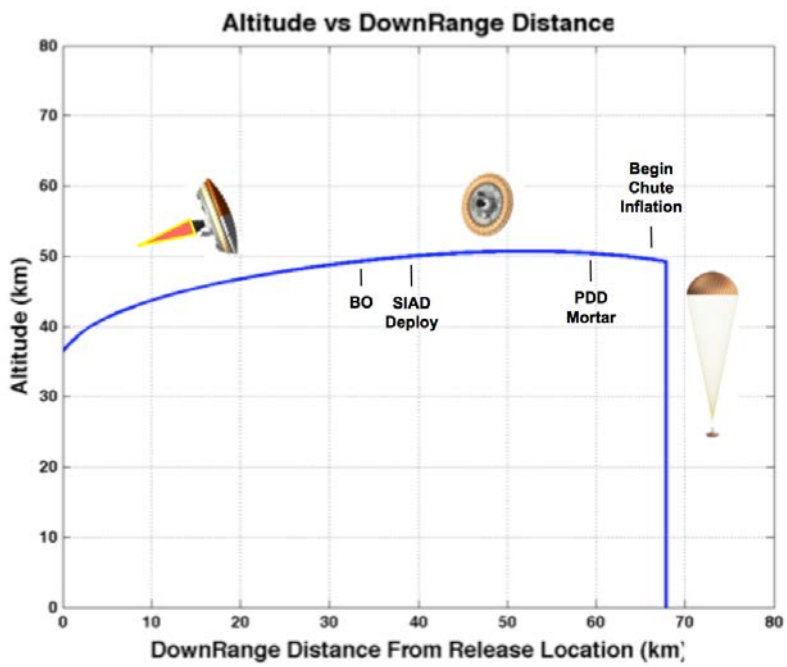

Figure 9: SFDT-1 Test Vehicle Altitude vs Down-Range Distance

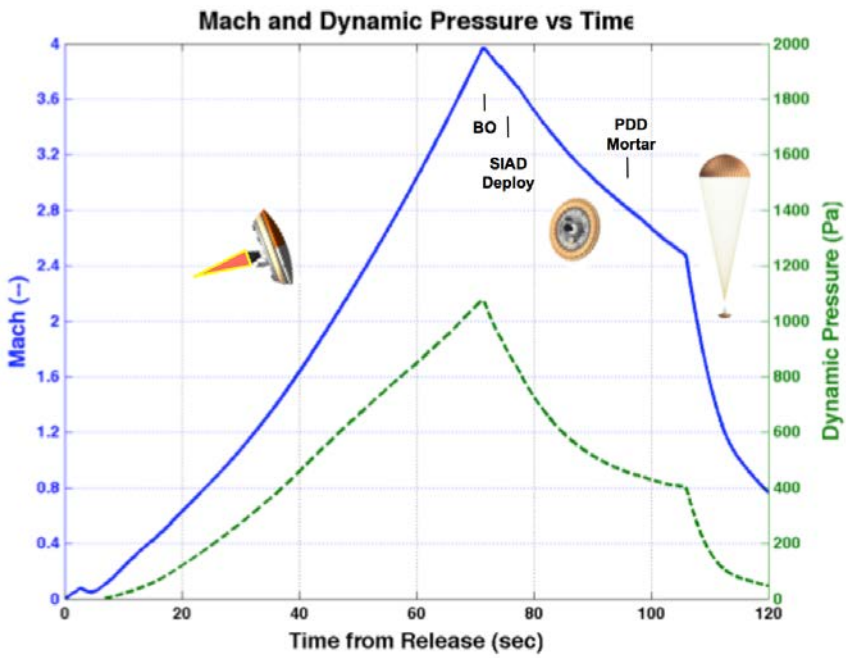

Figure 10: SFDT-1 Test Vehicle Mach and Dynamic Pressure vs Time

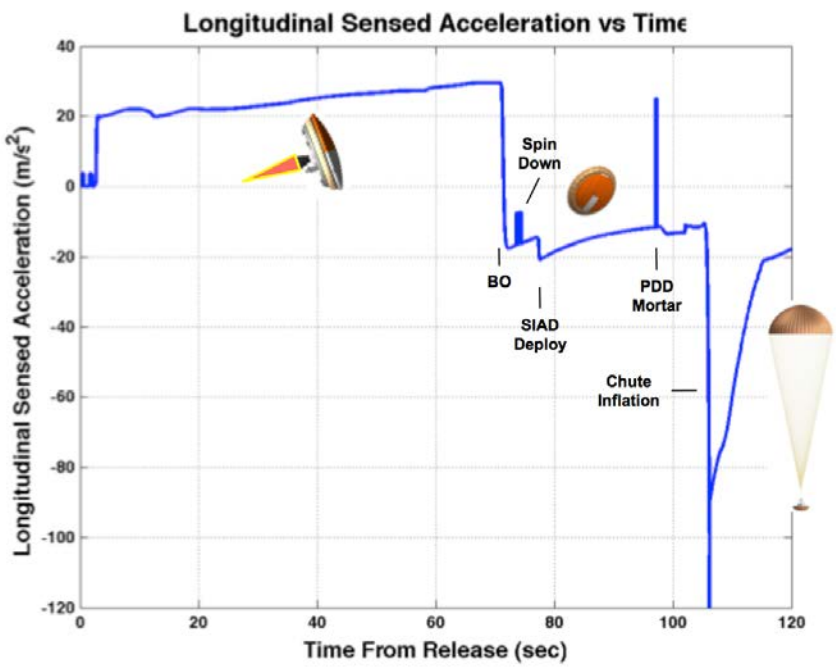

Figure 11: SFDT-1 Test Vehicle Sensed Acceleration vs Time

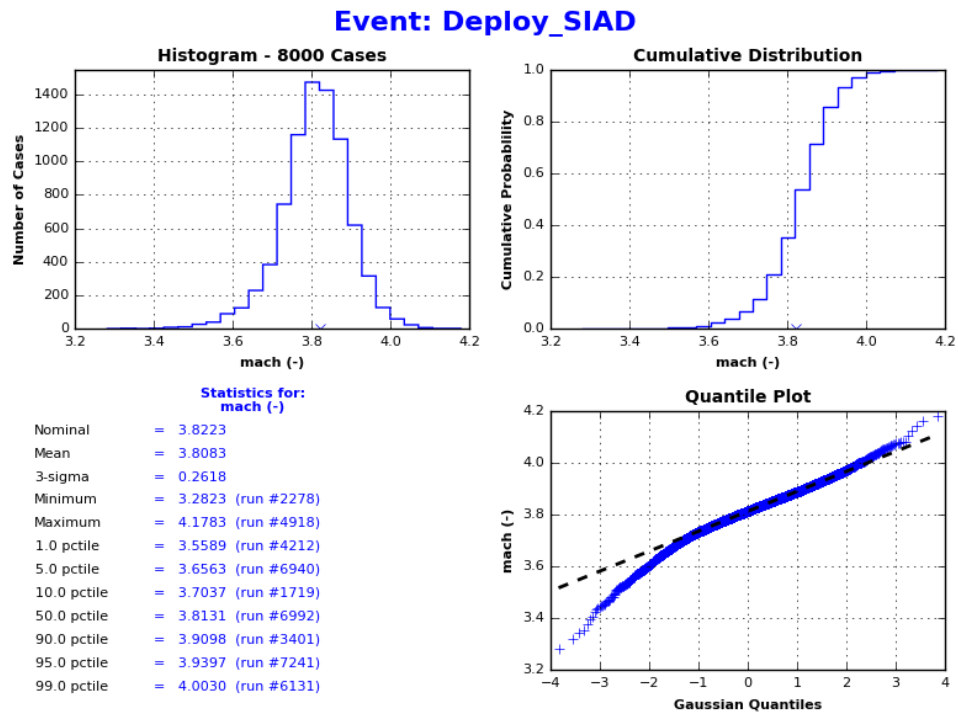

.

Figure 12: Uncertainty In Mach At SIAD Deployment

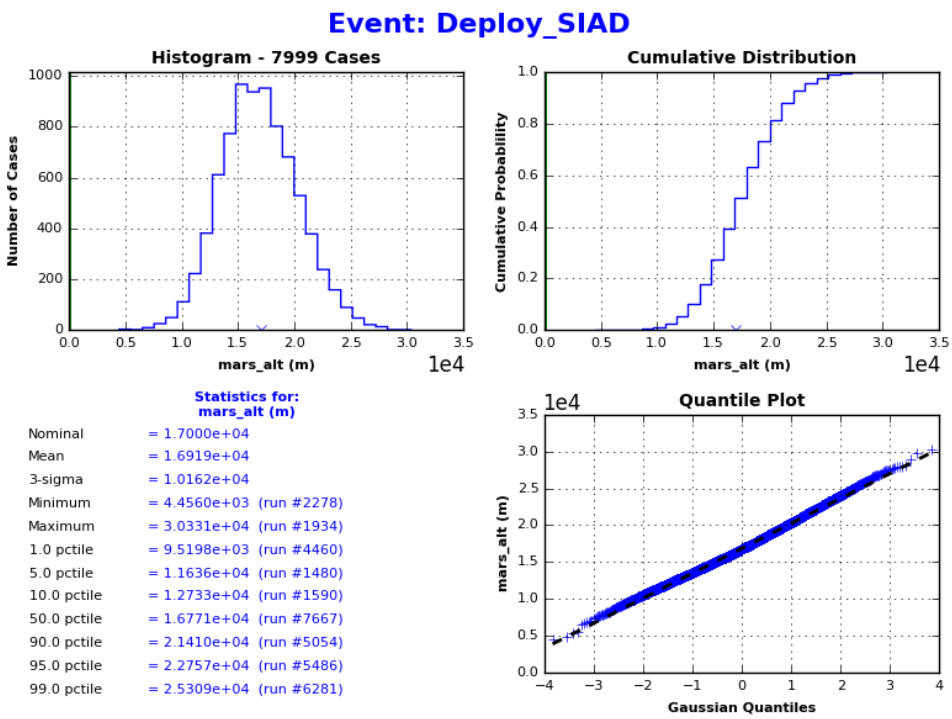

Figure 13: Uncertainty In Mars Altitude At SIAD Deployment

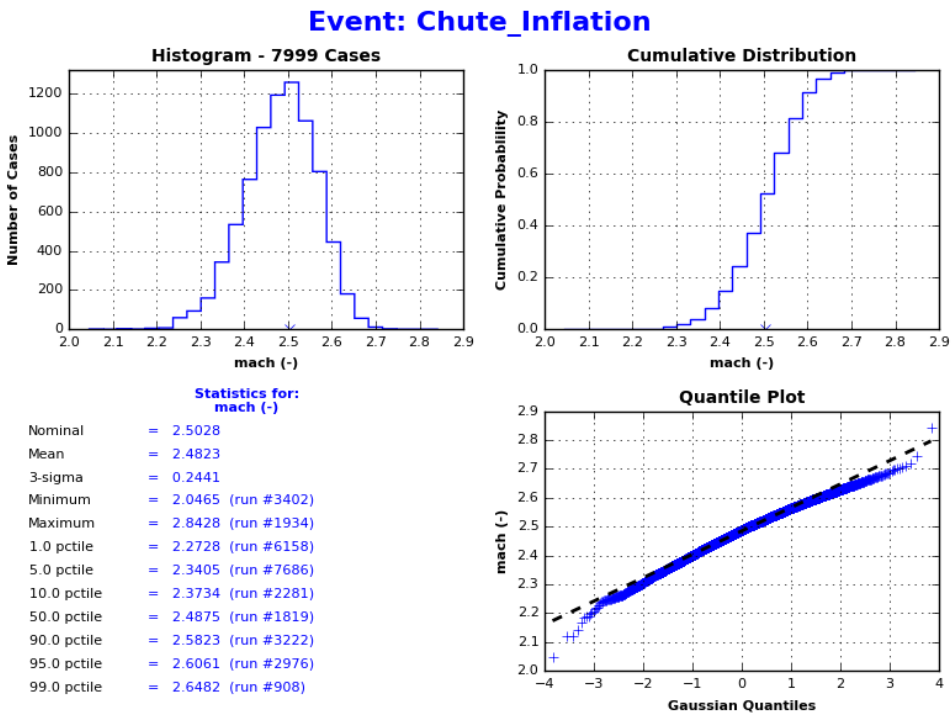

Figure 14: Uncertainty In Mach At Parachute Deployment

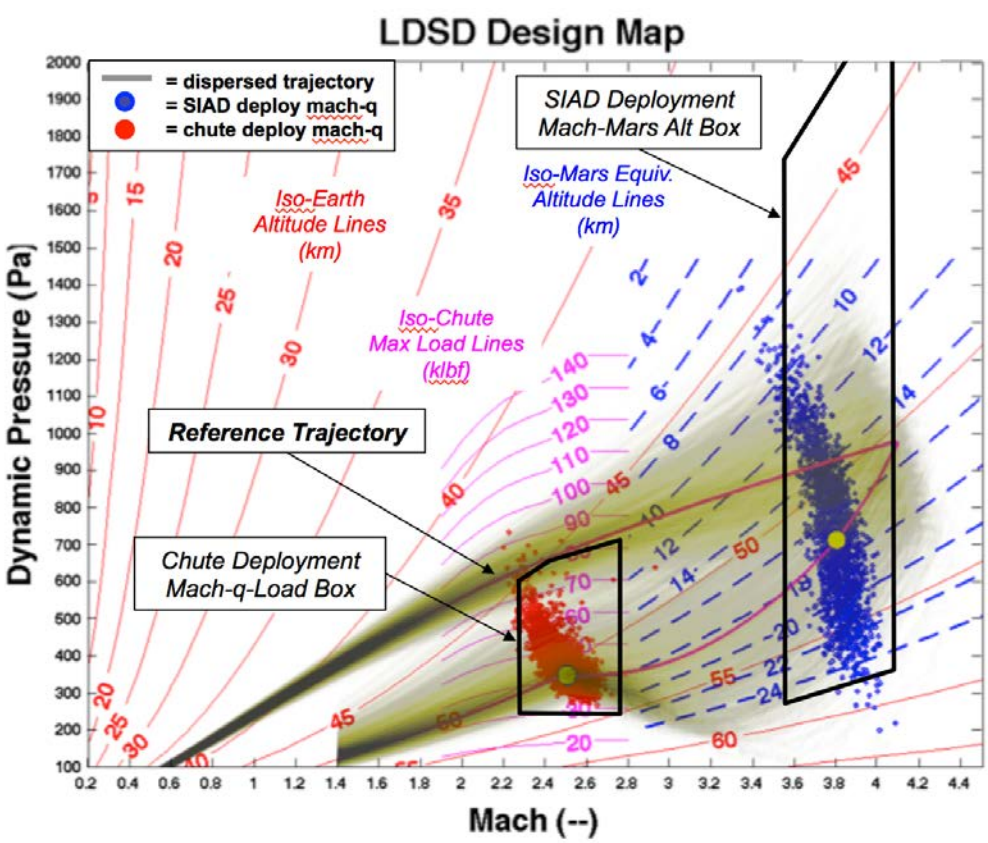

Figure 15: Uncertainty in Dynamic Pressure vs Mach with Environment Contours

V. On-Board Triggering Logic For SFDT-1

As part of the transition from pre-flight simulated trajectories to actual flight implementation, on-board software is typically created to provide the necessary sequencing of mission events. To this end, generalized flight software trigger logic was jointly designed specifically for LDSD by JPL and WFF with an architecture that enabled the end user to plug and play tailored triggering criteria. The trigger logic was implemented on a Gimbaled LN-200 with Miniature Airborne Computer (GLN-MAC), shown in Figure 16, manufactured by Sandia National Labs. The GLN-MAC includes a Northrop-Grumman (formerly Litton) LN-200 Inertial Measurement Unit (IMU) manufactured to the highest specifications for this type of unit. For SFDT-1, three main triggered events were required to accurately deploy the deceleration technologies to be tested: detection of Star48 burnout, speed to start the SIAD deployment sequence, and speed to start the parachute deployment sequence.

Figure 16: GLNMAC Flight Computer

An overview of the trigger state transition logic is depicted in Figure 17 and applies to any type of SFDT trigger. The triggering software is architected in two distinct and primarily independent logic paths: 1) the logic that governs the overall state of the trigger and 2) the logic that monitors the actual physical quantities unique to the trigger. Each logic path progresses through its own sequence of states all of which must be accomplished before the trigger can be confirmed met and subsequent action(s) taken. The transitions within the governing and physical monitoring paths from one state to the next are defined in Tables 4 and 5, respectively. Of particular note is the concept of a window of opportunity for the trigger to be accomplished. This opportunity window is defined by an earliest and latest time value enforced in the governing path. Time is used to define the window since trigger excursions outside of the window were considered most likely the result of a faulty sensor or navigation solution leaving time as the only functioning measurement in these cases.

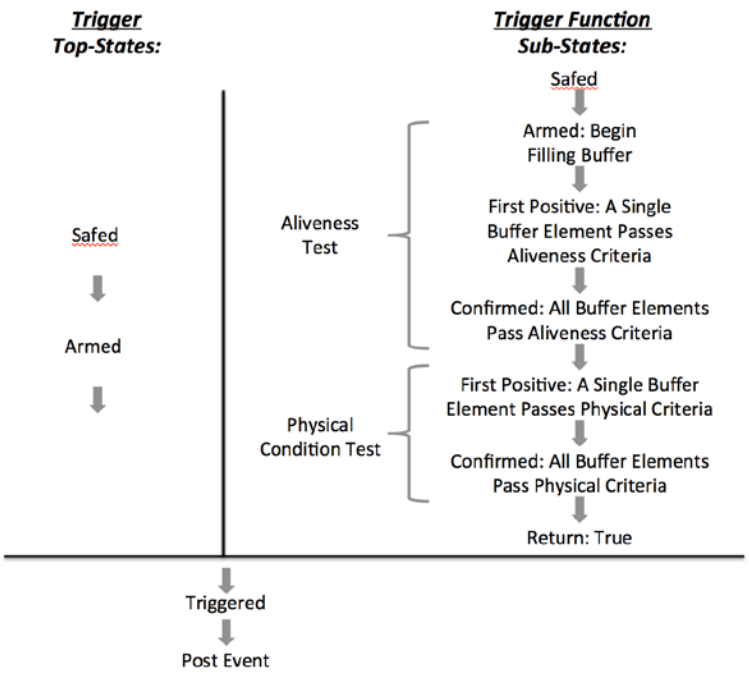

Figure 17: LDSD Generalized Trigger State Transition Design

Table 4: LDSD Governing Trigger State Transition Criteria

State Transition	Transition Description
Safed To Armed	Earliest time from the sensed drop from the balloon (or previous trigger). Trigger then becomes enabled and waits for the physical trigger criteria to be met.
Armed To Triggered	Occurs at either a not-to-exceed time from the sensed drop from balloon (or the previous trigger) or when the trigger value is met as confirmed by the phyiscal monitoring logic. The not-to-exceed time ensures transition of the mission sequence in the event the physical trigger does not meet the trigger criteria in a reasonable amount of time.
Triggered To Post Event	Occurs immediately after the trigger criteria is met and initiates sending of unique action discretes (e.g. SIAD deployment).

Table 5: LDSD Physical Trigger State Transition Criteria

State Transition	Transition Description
Safed To Armed	Time from the sensed drop from the balloon (or previous trigger). Software then begins to gather trigger related physical information into a buffer for evaluation.
Armed To 1st Positive ALIVENESS Buffer Element	Occurs when the 1st trigger related value that meets the ALIVENESS criteria is stored in the buffer. The ALIVENESS value is set to a magitude that ensures the trigger is receiving phyiscal quanities consistent with a heathly sensor.
1st Positive ALIVENESS Buffer Element To ALIVENESS Confirmed	Buffer has been filled with a sufficient number of phyiscal values to confirm integrity of sensor data.
ALIVENESS Confirmed To 1st Positive TRIGGER Buffer Element	Occurs when the 1st trigger related value that meets the TRIGGER criteria is stored in the buffer.
1st Positive TRIGGER Buffer Element To TRIGGER Confirmed	Buffer has been filled with sufficient number of physical values to confirm that the trigger criteria has been met. The monitoring logic sends a "True" indicator to the governing layer.

Referring back to Figure 11, the first software triggered inflight event was the detection of the Star48 burnout. Detection of the Star48 burnout was a necessary prerequisite for deploying any of the deceleration technologies. This was accomplished by monitoring the sensed acceleration from the IMU with burnout being confirmed after the thrust axis acceleration dropped below a user defined threshold value. During burnout the test vehicle transitions from positive thrust induced acceleration to negative drag induced deceleration. For SFDT-1, the thrust axis sensed acceleration criteria was set at the instant the thrust and drag forces cancelled each other. Subsequently by definition, the acceleration criteria was set to 0.0 m/s^2. Once accomplished, the burnout trigger enabled 1) the initialization of the reference time for the next trigger event (i.e. SIAD deployment) and 2) the sending of discrete signals to fire the spin down motors to remove the stabilizing spin rate required for the powered phase. The governing time window for the operation of the burnout trigger (i.e. min and max time) was set to a min time from drop consistent with a safe powered flight in the event the spin down motors were fired due to an erroneous burnout detection and a max time just beyond the max possible Star48 burn length. Recall from Table 4 that if the trigger criteria were not met by the time the window closes (i.e. the max time), the trigger logic would progress as if the criteria had been met.

The first deceleration technology to be deployed after the Star48 burnout was the SIAD. As mentioned previously, navigated speed was used as the triggering mechanism and for SFDT-1 was set to a value consistent with a Mach 3.8 condition at SIAD deployment (recall that altitude was not controlled inflight via the software but by the initial fixed hang angle while attached to the balloon). Since it was required to deploy the SIAD after the powered phase, the reference time used in the SIAD trigger logic was from detection of Star48 burnout. Recall that the spin down of the vehicle occurred right after burnout detection (Table 2) and was required to be complete prior to deployment of the SIAD. Through the sensitivity studies, it was evident that the variation in speed at Star48 burnout might produce a condition such that SIAD deployment could occur immediately after the spin down phase (i.e. no coasting prior to deploying the SIAD). Therefore the governing time window for the operation of the SIAD trigger was set such that the minimum time was immediately following spin down to a max time consistent with the max time of SIAD deployment as evident from Monte Carlo analysis.

The second and final deceleration technology to be deployed was the parachute. Again, navigated speed was used as the triggering mechanism and for SFDT-1 was set to a value consistent with a Mach 2.5 condition at parachute line stretch (i.e. the start of inflation). Since deployment of the SIAD was a necessary prerequisite for deploying the parachute (i.e. one main objective was to observe dynamics of the parachute behind a blunt body with a deployed SIAD), the reference time used in the parachute trigger logic was from deployment of the SIAD. Sensitivity studies showed a large variation in the timing of when the parachute speed trigger would be met after SIAD deployment due to the uncertainties earlier during the powered phase. Therefore defining a min and max window of time for the deployment of the parachute required more thought than the deployment of the SIAD. Defining the minimum time was somewhat easier and was informed by the requirement that the trajectory enable at least 10sec of SIAD deployed free flying test time (Table 1). This min test time requirement was met statistically so the minimum time was set to 5sec as a absolute minimum in the event dispersions were greater than those investigated. The max time considered two primary scenarios: 1) the possible deployment conditions if the navigation solution became corrupted and the parachute was deployed not at the correct deployment criteria but at the max time and 2) the deployment condition if navigation solution was operating correctly but the trigger still deployed on the max time due to a long yet valid coast time necessary achieve the correct deployment criteria. Both scenarios were treated with equal likelihood albeit both were considered bounding cases. The max time was determined to be the value that balanced all the possible negative consequences (e.g. chute extraction low/high dynamic pressure, chute inflation low/high Mach, and low/high chute loads).

VI. SFDT-1 As-Flown Trajectory

At 8:40:51am HST on June 28, 2014 the balloon with the SFDT-1 flight vehicle attached lifted off from PMRF. At 11:05:00am HST later that day the SFDT-1 flight vehicle was released from the balloon at an altitude of ~36km and with splashdown occurring at ~11:25:00am HST (Figures 18 and 19). The achieved as-flown flight conditions are listed in Table 6.

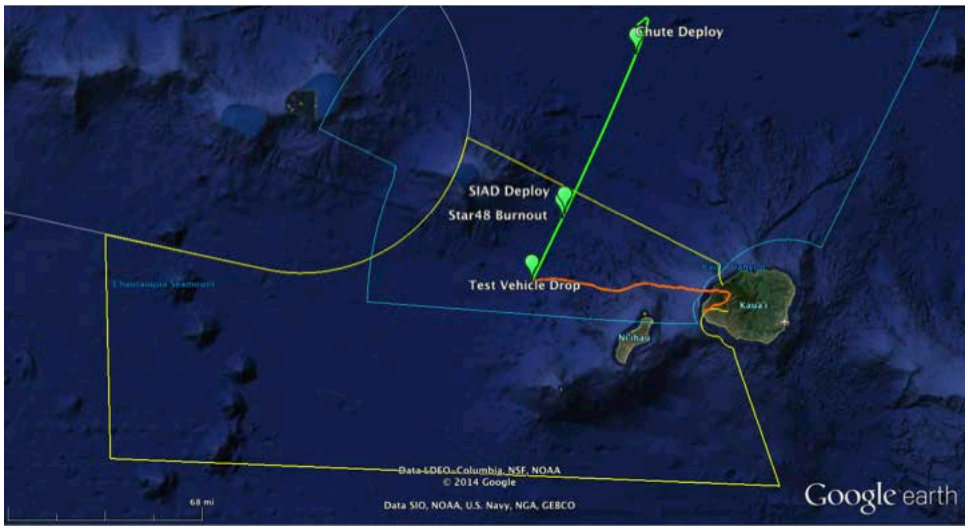

Figure 18: LDSD Balloon (orange) and Test Vehicle (green) Ground Trace

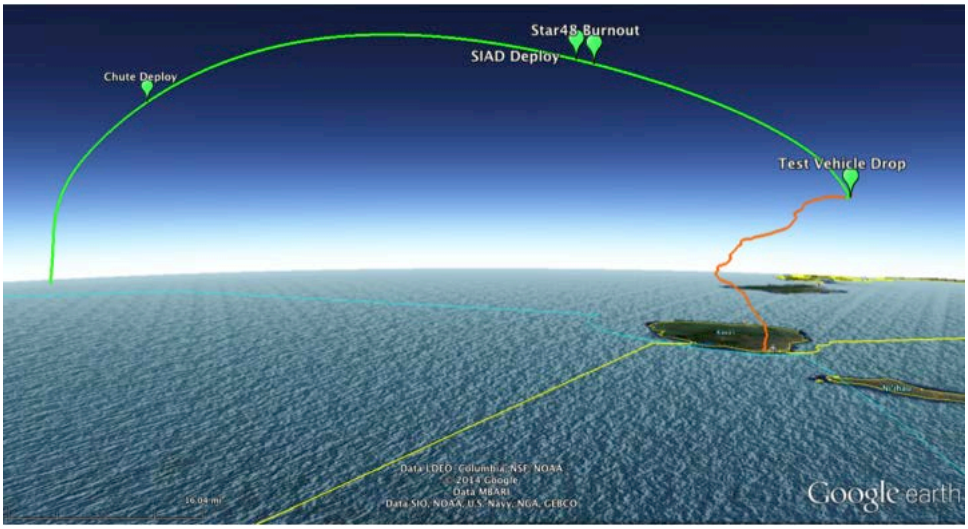

Figure 19: LDSD Balloon (orange) and Test Vehicle (green) Trajectories

Table 6: SFDT-1 As-Flown Trajectory Parameters

Flight Requirements	Predicted Value	As Flown
SIAD Deploy Mach ***Target***	3.8	4.08 +/- 0.09
SIAD Chute Line Stretch Mach ***Target***	2.5	2.54 +/- 0.05
SIAD Deploy Scaled Mars Altitude ***Target***	17km	25.8 +/- 0.2km
SIAD Deploy Mach Error	+/- 0.25	4.08 +/- 0.09
Chute Line Stretch Mach Error	+/- 0.25	2.54 +/- 0.05
Min Dynamic Pressure At Chute Line Stretch	>= 240 Pa	545 Pa
Max Chute Inflation Load	<= 80 klbf	--
Max AoA From SIAD Deploy To Chute Line Stretch	<= 25 deg	25.005 +/- 0.06 deg
SIAD Deployment Max Dynamic Pressure	<= 2000 Pa	330 Pa
Max Residual Spin Rate After Spin Down	<= 20 deg/sec	2.87 deg/sec
Max AoA From SIAD Deploy To PDD Trigger	<= 20 deg	2.75 deg/sec
Max Delta Density From SIAD Deploy to SIAD Deploy + 10 sec	<= 10^{-4} kg/m^3	10^{-5} kg/m^3
Min Time From SIAD Deploy to PDD Trigger	>= 10 sec	85.95 sec

All flight sequenced activity listed in Table 2 performed as designed however the test vehicle departed from the planned trajectory achieving a higher sub-orbital arc compared to the nominal (Figure 20). The lofted trajectory had a number of physical consequences that are listed in Table 7.

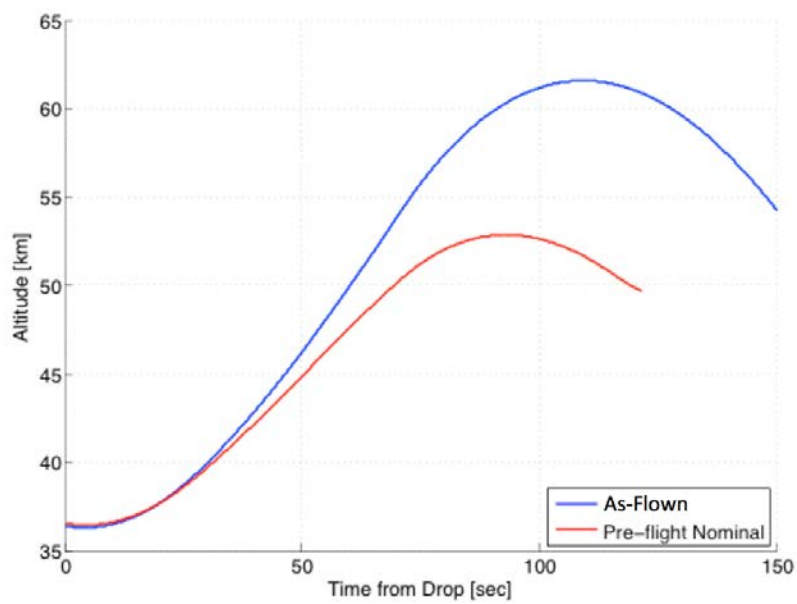

Figure 20: As-Flown and Pre-flight Predicted SFDT-1 Altitude vs Time

Table 7: Consequences and Rationale of a Higher Than Expected SFDT-1 Flight Profile

Observation	Rationale
High SIAD deployment altitude	Due to the lofted trajectory
High SIAD deployment Mach	Lofted trajectory lead to lower speed of sound which lead to higher Mach number at the triggered speed
Lower SIAD deployment dynamic pressure	Lofted trajectory lead to lower atm density leading to lower dynamic pressure
Long time from SIAD deployment to parachute deployment	Lofted trajectory lead to lower atm density leading to lower drag which lead to longer deceleration time
Steeper flight path angle at parachute deployment	Lofted trajectory lead to more extensive gravity induced turning of the velocity vector prior to deployment
Higher dynamic pressure at parachute deployment	Steeper flight path angle lead to a deeper penetration into higher density atmosphere which lead to higher dynamic pressure

Post flight reconstruction was conducted on the entire test vehicle flight phase with a concentration on the root cause of the off-nominal trajectory. After extensive analysis it was concluded that two main contributors were responsible for the lofted SFDT-1 trajectory. First, the aerodynamic moment coefficients during the transonic phase of powered flight were determined to be lower than predicted (i.e. trimming torque was less than predicted). As discussed earlier in the paper, the trajectory was known to be sensitive to uncertainty in the transonic moment coefficients and the effect was consistent with that sensitivity. Second, the Star48 solid rocket motor was determined to have higher than predicted thrust early during the powered phase. As a consequence, the test vehicle accelerated to higher altitudes quicker than predicted, leading to lower density atmospheric flight which lead to lower dynamic pressure which finally lead to lower trimming torque causing the vehicle to propel itself to higher altitudes. Modeling adjustments were made both in the powered phase aerodynamic moment coefficients as well as the Star48 ballistics to account for the observations in SFDT-1 and will be utilized for SFDT-2 (Ref 6).

VII. Summary

This paper presented the interaction of the hardware and vehicle performance design cycles that lead to final SFDT-1 flight configuration. SFDT-1 test vehicle performance assessment methods using the JPL simulation tool DSENDS were also discussed along with subsequent identification of trajectory sensitivities. Development of a mission sequence and the on-board triggering logic were discussed including considerations for the development of the SFDT-1 triggering flight constants. Finally, the as-flown SFDT-1 trajectory performance was discussed with explanation of the observed off-nominal altitude performance.

References

[1]Ian G. Clark, Mark Adler, and Tommaso P. Rivellini, “Development and Testing of a New Family of Supersonic Decelerators,” Aerodynamic Decelerator Systems Conference, 2013.

[2]Juan R. Cruz, “*Nondimensional Scaling of Aerodynamic Decelerator Tests*,” Presentation and associated Appendices from the 9th AIAA Aerodynamic Decelerator Systems Technology Seminar, 1986.

[3]Rob Grover, “Entry, Descent and Landing Systems Analysis Study: Phase 2 Report on Mars Science Laboratory Improvement,” NASA/TM-2011-216988, 2012

[4]Brant T. Cook, Guillermo Blando, Andrew Kennett, Max Von Der Heydt, John Luke Wolff, and Mark Yerdon,”High Altitude Supersonic Decelerator Test Vehicle,”

[5]John Van Norman, ”Aerodynamic Models for the Low Density Supersonic Decelerator (LDSD) Supersonic Flight Dynamics Test (SFDT),” Aerodynamic Decelerator Systems Conference, 2015

[6]E. Blood et al, “LDSD Supersonic Flight Dynamics Test 1: Post-flight Reconstruction,” IEEE Aerospace Conference, 2015

[7]J. Balaram, R. Austin, P. Banerjee, T. Bentley, D. Henriquez, B. Martin, E. McMahon, G. Sohl, "*DSENDS - A High-Fidelity Dynamics and Spacecraft Simulator for Entry, Descent and Surface Landing*", **IEEE 2002 Aerospace Conf.**, Big Sky, Montana, March 9-16, 2002.

[8]Bowes, A.L., et al., "LDSD POST2 Simulation and SFDT-1 Pre-Flight Launch Operations Analyses", AAS Paper 15-232, 25th AAS/AIAA Space Flight Mechanics Meeting, Williamsburg, VA, January 11-15, 2015.

Acknowledgement

The research was carried out at the Jet Propulsion Laboratory, California Institute of Technology, under a contract with the National Aeronautics and Space Administration.